

## ARTICLES

## Thermodynamic Stability and Melting Mechanism of Bimetallic Au–Pt Nanoparticles

H. B. Liu,<sup>†</sup> U. Pal,<sup>\*,‡</sup> and J. A. Ascencio<sup>§</sup>

*Instituto Mexicano del Petróleo, Eje Central Lázaro Cárdenas No. 152, Col. San Bartolo Atepehuacan, C.P. 07730, Mexico D.F., Mexico; Instituto de Física, Universidad Autónoma de Puebla, Apdo. Postal J-48, Puebla, Puebla 72570, Mexico; and Instituto de Ciencias Físicas, Universidad Nacional Autónoma de México, AP 48-3, Cuernavaca 62210, Morelos, Mexico*

*Received: April 1, 2008; Revised Manuscript Received: September 11, 2008*

Classical molecular dynamics simulations were carried out to study the thermodynamic stability and melting behavior of Au–Pt nanoclusters of most common structural variants like decahedra, icosahedra, and cuboctahedra. It has been shown that the Pt-core/Au-shell structures are most stable, while the eutectic-like structures are more stable than solid solution ones, and the Au-core/Pt-shell are least stable, on thermal heating. On the other hand, the large difference between the melting points of the constituent elements can be a dominating factor on the melting mechanism of the bimetallic nanoparticles. The bimetallic clusters transform to the most stable Pt-core/Au-shell structure from whatever initial structures on heating above certain temperatures.

## I. Introduction

Au–Pt bimetallic nanoparticles are of special interest for their applications in catalysis, specially for electrocatalysis in fuel cell reactions, such as methanol oxidation<sup>1,2</sup> and electrocatalytic reduction of oxygen.<sup>3,4</sup> Recently bimetallic Au–Pt nanoparticles with different compositions, sizes, structures, and morphologies have been synthesized.<sup>1–10</sup> For practical applications, adequate knowledge of their structural stability and thermodynamic behavior are of immense importance. For bulk Au–Pt system, there is a miscibility gap for a large range of composition and temperature,<sup>11,12</sup> which might have a great influence on the characteristics of their nanoparticles. On the other hand, Au–Pt nanoparticles might have different properties from the binary alloy systems with strong chemical order such as Au–Pd,<sup>13</sup> Au–Cu,<sup>14</sup> and Ni–Ti.<sup>15</sup> Au–Pt bimetallic nanoparticles were found to display alloy properties,<sup>5</sup> which is in sharp contrast to its bulk bimetallic miscibility gap for a large range. On the other hand, their core/shell structures were comprehensively synthesized and studied by several researchers.<sup>6–10</sup> In those studies, Au-core/Pt-shell particles were frequently prepared by controlling the synthesis conditions.

In the present study, structural analysis of a variety of Au–Pt nanoclusters was performed theoretically in order to reveal the thermodynamic and dynamic stability of the structures as well as their melting mechanisms.

## II. Simulation Methods

For the molecular dynamics simulation, interatomic interactions between Au and Pt were described by a simple analytical

embedded-atom method (EAM) developed by Cai et al.<sup>16</sup> The model includes a long-range force. In this model, electron-density function is taken as decreasing exponential function; two-body potential is defined as a function given by Rose et al.<sup>17</sup> and embedding energy is assumed to be a universal form as suggested by Banerjee and Smith.<sup>18</sup> The alloy model of Johnson<sup>19</sup> is applied and an extra parameter is introduced in order to fit dilute-limit heats of solution. For three possible compositions AuPt<sub>3</sub>, AuPt, and Au<sub>3</sub>Pt, the predicted heats of formation are in reasonable agreement with first-principles calculations and experimental data, and consistent lattice constants are predicted. The Au–Pt alloying potential can be used for a wide range of components with a high accuracy. The MD simulations were performed using XMD developed by J. Riffkin.<sup>20</sup> The program employs a predictor–corrector algorithm to integrate the equation of motion. The MD simulations were considered as converged when the energy changes were less than  $1 \times 10^{-7}$  eV for a relatively long time ( $\sim 10^{-8}$  s).

## III. Results and Discussion

**A. Structural Stability.** In order to study the structure and composition profiles of the Au–Pt bimetallic nanoclusters as small as 2–3 nm, three of their most common geometrical configurations were constructed. They are 309-atom cuboctahedron, 262-atom decahedron, and 309-atom icosahedron. It must be noted that the clusters under study are too large to apply exhaustive search techniques. Therefore, we just selected the above-mentioned three types of clusters, which are most commonly observed in experiment,<sup>21</sup> and relaxations were performed at 0 K for a long time. Three possible types of elemental distribution namely eutectic-like, solid solution, and core/shell are studied. The specific compositions are Au<sub>147</sub>Pt<sub>162</sub> and Pt<sub>147</sub>Au<sub>162</sub> for 309-atom cuboctahedra and icosahedra, Au<sub>99</sub>Pt<sub>163</sub> and Pt<sub>99</sub>Au<sub>163</sub> for 262-atom decahedra. Two possible types of core/shell structures, Au-core/Pt-shell and Pt-core/Au-

\* Corresponding author. E-mail: upal@sirio.ifuap.buap.mx. Fax: +52-222-2295611.

<sup>†</sup> Instituto Mexicano del Petróleo.

<sup>‡</sup> Universidad Autónoma de Puebla.

<sup>§</sup> Universidad Nacional Autónoma de México.

**TABLE 1: Formation Energies of Au–Pt Bimetallic Cubooctahedral Clusters with 309 Atoms, at 0 K**

Morphology	Type of structure	component	Total cohesive energy per atom, eV	Total formation energy of bimetal, eV
	Pure Au	309 Au 0 Pt	-3.9070	0
	Pure Pt	0 Au 309 Pt	-5.7305	0
	Eutectic-like	147 Au 162 Pt	-4.8756	-3.8869
	Eutectic-like	162 Au 147 Pt	-4.7831	-2.6533
	Solid solution	147 Au 162 Pt	-4.8331	9.2452
	Solid solution	162 Au 147 Pt	-4.7453	9.0190
	Au-Core/Pt-shell	147 Au 162 Pt	-4.7319	40.5247
	Pt-Core/Au-Shell	162 Au 147 Pt	-4.8494	-23.1481

shell are considered with single-layer atomic shells of specific composition. None of the nanoclusters was a dilute solution either of Au or of Pt, in order to fall squarely within the immiscibility gap. The model structures for the cubooctahedral, decahedral, and icosahedral geometries are shown in the Tables 1, 2, and 3, respectively. From the structural images, the elemental distributions in the bimetallic nanoclusters can be seen clearly. Their three-dimensional geometrical structures can be seen in our previous work.<sup>21</sup> For each model cluster,  $3.2 \times 10^7$  time steps of  $2 \times 10^{-15}$  s each were run at 0 K. The long simulation time ensured the relaxation of the initial configurations to their local minima. These minima are described by energy changes not exceeding  $1 \times 10^{-7}$  eV in magnitude and thus can be considered stationary points on the potential energy surface. The error of the potential we used was 0.05%.<sup>16</sup> The used integration algorithm for the equation of motion was a high-precision fifth-order Gear predictor–corrector, and the time steps were relatively small for the pure Au and Pt clusters, at 0 K. Usual test of precision of the algorithm is the variation of the root mean square of the total energy over a number of steps. From the statistical variation of our simulated results, it has been observed that the precision of the obtained results is much higher than that of the potential we used. Therefore, the systematic error in the calculated energy is limited to that of the potential: about 0.05%. In general, the calculated energies presented in the Tables 1, 2, and 3 are of same order of precision.

The formation energy was calculated from the difference of the cohesive energies between the alloy and its pure components.<sup>13</sup> The formation energies of the Au–Pt bimetallic cubooctahedral clusters with 309 atoms at 0 K are shown in Table 1. It can be seen that the total formation energies of Pt-core/Au-shell and eutectic-like clusters are negative, which demonstrates that they are thermodynamically favorable. Solid solution and Au-core/Pt-shell clusters have positive energies. The stability order for the bimetallic clusters is: Pt-core/Au-shell > eutectic-like > solid solution > Au-core/Pt-shell.

The formation energies of Au–Pt bimetallic decahedral clusters with 262 atoms are shown in Table 2. The stability order in this case is consistent with the cubooctahedra, except

**TABLE 2: Formation Energies of Au–Pt Bimetallic Decahedral Clusters with 262 Atoms, at 0 K**

Morphology	Type of structure	component	Total cohesive energy per atom, eV	Total formation energy of bimetal, eV
	Pure Au	262 Au 0 Pt	-3.8949	0
	Pure Pt	0 Au 262 Pt	-5.7049	0
	Eutectic-like	99 Au 163 Pt	-5.0161	1.2780
	Eutectic-like	163 Au 99 Pt	-4.5707	2.1156
	Solid solution	99 Au 163 Pt	-4.9705	13.2142
	Solid solution	163 Au 99 Pt	-4.5429	9.4144
	Au-Core/Pt-shell	99 Au 163 Pt	-4.9098	29.1152
	Pt-Core/Au-Shell	163 Au 99 Pt	-4.6406	-16.2049

the formation energies of eutectic-like clusters are a slight positive.

The formation energies of the Au–Pt bimetallic icosahedral clusters with 309 atoms are shown in Table 3. Again, we can see that their stability order is consistent with cubooctahedra and decahedra clusters. The eutectic-like clusters have positive energy as decahedra.

From the point of view of geometrical structure, the core/shell icosahedra and cubooctahedra have similar stabilities, while eutectic-like and solid solution-like cubooctahedra are better stable than the same type of icosahedra. As the decahedra have different number of atoms in comparison with cubooctahedra and icosahedra, their stability cannot be compared directly, even by the average formation energy per atom.

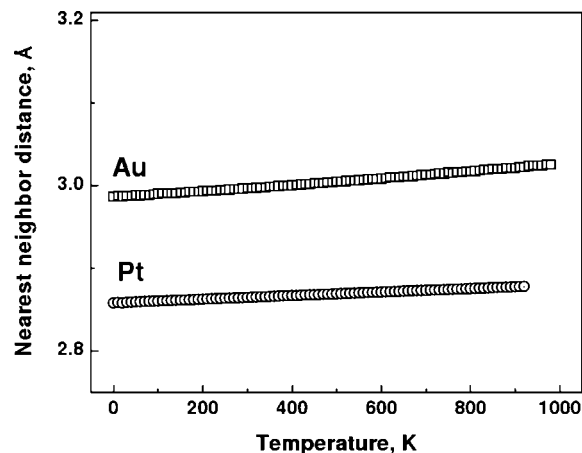
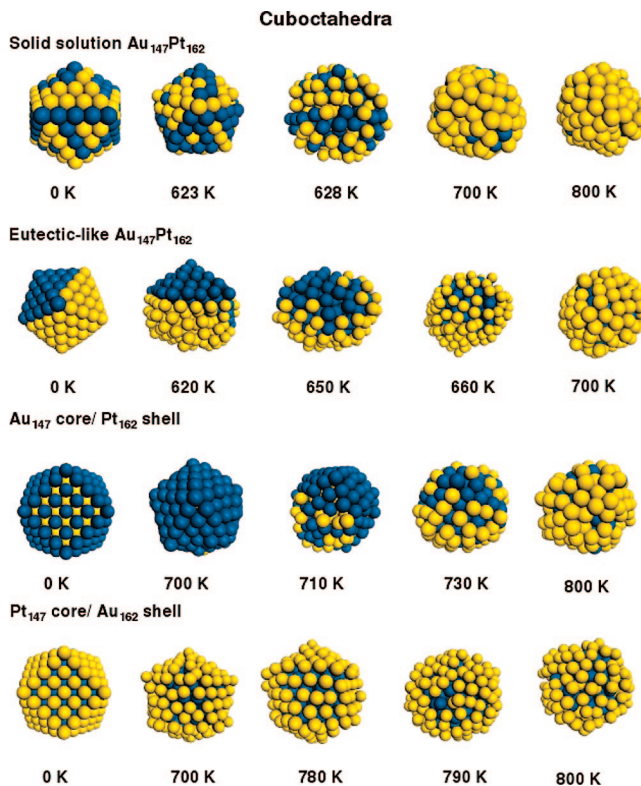
In general, from the viewpoint of elemental distribution, the stability order is consistent for all three types of structures; Pt-core/Au-shell is most stable, and then eutectic-like, solid solution, and Au-core/Pt-shell. Presumably, two factors decide the stability of the bimetallic nanoclusters: chemical order and structural incoherency. From the Au–Pt phase diagram,<sup>11,12</sup> it can be seen that there is no intermetallic compound phase; in contrast, there is a wide immiscibility gap for a certain temperature range. At low temperature range, Au–Pt may be in different solid solutions or mixture of solid solution and pure metal. That is to say, chemical order between Au and Pt atoms is weak and hence is not favorable to form alloy structures. Both core/shell and eutectic-like structures are not alloys by nature. As for the structural incoherence, the nearest-neighbor distances for Au and Pt are 2.88 and 2.77 Å,<sup>22</sup> respectively. Clearly, Au has a larger nearest-neighbor distance than Pt. Considering the surface contraction effect of the cluster, the Pt-core/Au-shell structure will accommodate better than their reverse structure Au-core/Pt-shell, as the larger Au–Au separation decreases by surface contraction effects, yielding a better lattice matching between Pt and Au. The bulk Au–Pt with the similar composition to the solid solution clusters under study remains as the mixture of two different components of crystalline solid solutions. However, the structural incoherency in cluster solid solution should be larger than in the crystalline solid

**TABLE 3: Formation Energies of Au–Pt Bimetallic Icosahedral Clusters with 309 Atoms, at 0 K**

Morphology	Type of structure	component	Total cohesive energy per atom, eV	Total formation energy of bimetal, eV
	Pure Au	309 Au 0 Pt	-3.9198	0
	Pure Pt	0 Au 309 Pt	-5.7543	0
	Eutectic-like	147 Au 162 Pt	-4.8723	2.8696
	Eutectic-like	162 Au 147 Pt	-4.7861	1.9704
	Solid solution	147 Au 162 Pt	-4.8287	16.3430
	Solid solution	162 Au 147 Pt	-4.7493	13.3534
	Au-Core/Pt-shell	147 Au 162 Pt	-4.7544	39.3069
	Pt-Core/Au-shell	147 Au 162 Pt	-4.8670	-23.0263

solution on per volume or per atom basis, which makes the cluster unstable. The above analysis indicates that the incoherency has greater effect on structure formation than the weak chemical ordering. Therefore, the stability of the final structures is determined mainly by structural incoherency. Note that if there were a crossing of nearest-neighbor distances with temperature, then the structural incoherence would predict a different stable structure above that temperature. However, the experimental thermal expansion coefficients of bulk Au and Pt are  $3.556 \times 10^{-5}$  cm/K and  $2.286 \times 10^{-5}$  cm/K at 20 °C, respectively.<sup>22</sup> That is to say, Au has larger nearest-neighbor distance and larger thermal expansion coefficient. Therefore, there is no cross on nearest-neighbor distances for bulk Au and bulk Pt with the increase of temperature. To underscore this point, we also performed simulations within the constant pressure and constant temperature ensemble to predict the nearest-neighbor distances of Au and Pt, both fcc crystals. Our simulated nearest-neighbor distances of Au and Pt are in good agreement with the reported experimental data; and there is no crossing of nearest-neighbor distances for a wide range of temperatures (Figure 1). This point is reinforced in the next section by analyzing the structural transformations during heating.

**B. Melting Mechanism and Structural Features at High Temperatures.** It can be seen from the phase diagram that the Au–Pt phase composition changes greatly with temperature.<sup>11,12</sup> Therefore, the dynamic stability and melting mechanism of the Au–Pt bimetallic nanoparticles are expected to be affected with the variation of composition. To address this possibility, a series of heating processes was performed from 0 to 1500 K at the rate of  $5 \times 10^{11}$  K/s, increasing the temperature linearly. Structural transformations of Au-core/Pt-shell, eutectic-like, and solid solution cuboctahedral clusters during heating are visualized in Figure 2 for some discrete temperatures. At 0 K, the solid solution  $\text{Au}_{147}\text{Pt}_{162}$  cuboctahedral cluster has random elemental distribution and regular cuboctahedral geometry. On heating up to 623 K, the atomic arrangements at the corners become a little disordered and the cluster loses its regular shape at 628 K. At 700 K, it can be observed that the Au atoms occupy more surface sites, and almost fill-up all surface sites at about

**Figure 1.** Simulated nearest-neighbor distances of Au and Pt, both FCC crystals versus temperatures.**Figure 2.** Structural transformations of Au-core/Pt-shell, eutectic-like, and solid solution clusters during heating processes.

800 K, forming Pt-core/Au-shell liquid cluster. The precise melting temperatures of the clusters can be followed from the Figures 3 and 4. For eutectic-like  $\text{Au}_{147}\text{Pt}_{162}$  cuboctahedral cluster, the image at 0 K shows its initial elemental distribution. On heating up to 620 K, the low melting point Au ( $1337 \text{ K}^{22}$ ) starts to melt and the cluster becomes disordered. The image at 650 K displays clearly the process of Au covering over the unmelted, high melting point Pt part ( $2041 \text{ K}^{22}$ ). At about 660 K, the whole cluster changes to rounded shape with Au on the surface. Up to 700 K, the molten cluster has similar structure as of solid-solution cluster at 800 K. For  $\text{Au}_{147}$ -core/ $\text{Pt}_{162}$ -shell cuboctahedral cluster, on heating up to 700 K, the atomic arrangements at the corners become a little disordered. The cluster loses its regular shape at about 710 K, while Au atoms start to segregate toward the surface. At about 730 K, most of the Au atoms occupy the surface sites, and the cluster starts to melt. At about 800 K, it becomes a Pt-core/Au-shell liquid

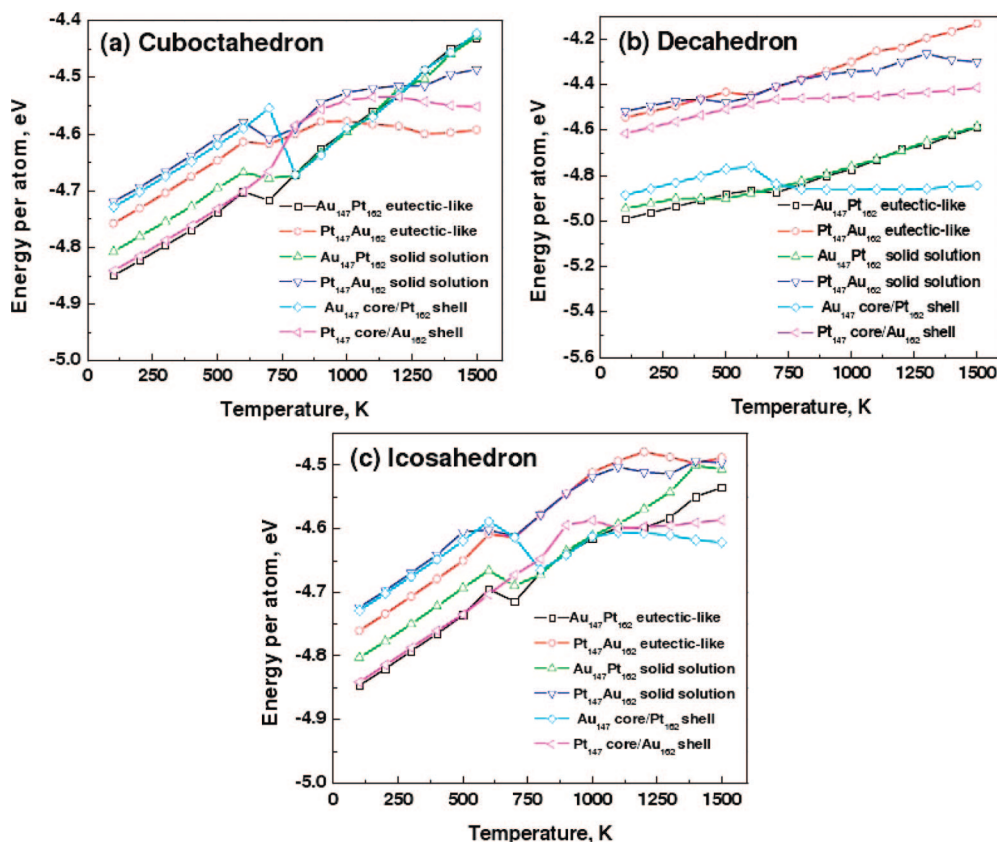


**Figure 3.** Dependence of energy per atom and temperature during heating process of (a) cuboctahedra, (b) decahedra, and (c) icosahedra.

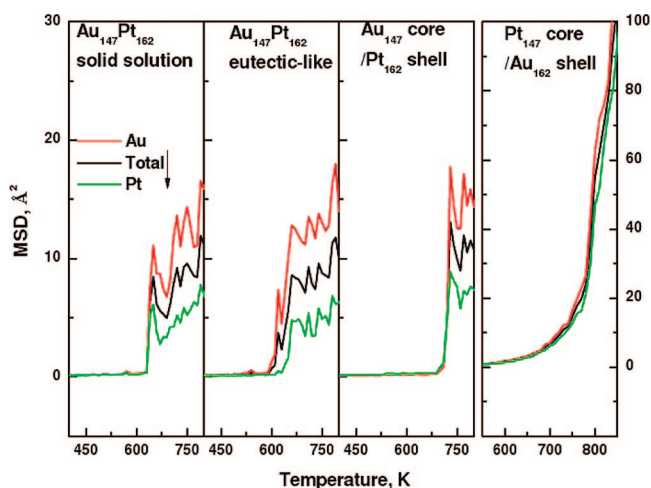


**Figure 4.** Mean square displacements (MSD) versus temperature during heating for cuboctahedra.

cluster. For the  $\text{Pt}_{147}\text{-core}/\text{Au}_{162}\text{-shell}$  cuboctahedral cluster, on heating up to 700 K, the atomic arrangements at the corners become a little disordered and the cluster keeps its basically regular shape till 780 K. The cluster starts melting in between 790 and 800 K.

Summarizing the above observations, it seems that the huge difference between the melting points of Au and Pt has a great influence on the melting mechanism of the Au–Pt bimetallic clusters. From the melting process of Pt-core/Au-shell cluster, it can be seen that the stabilizing effect of high melting point Pt-core on the whole cluster structure is very apparent. While for Au-core/Pt-shell structure, Pt has similar effect, resulting in the melting point of the cluster higher than the solid solution and eutectic-like structures. For the Au-core melting, the Pt-

shell loses its stability rapidly. For eutectic-like clusters, the coexistence of disordered Au and order Pt is also evident. From the point of view of structure transformation, the heating process transforms whatever structures to the most stable Pt-core/Au-shell structure at certain temperatures (see the images at highest temperatures for each structure in Figure 2).

Melting processes of decahedra and icosahedra were also studied. However, their melting processes are similar to that of cuboctahedra, and hence are not presented.

To analyze the above-mentioned structural transformations from the point of view of phase transformation, the variation of total energy per atom with temperature during the heating process is studied for the considered structures. The total energy includes binding energy and kinetic energy. The results are plotted in Figure 3 for all the bimetallic clusters under study.

The dependences of energy per atom and temperature during heating process of cuboctahedra, decahedra, and icosahedra bimetallic clusters are plotted in Figure 3, a, b, and c, respectively. Pt-core/Au-shell cuboctahedron and icosahedron show the features of nonequilibrium melting, with an uphill step between solid and liquid sides due to a finite heat of fusion. The rest of the clusters exhibit different irregular melting patterns. In comparison with the regular nonequilibrium melting (phase transformation), all the irregular melting processes include extra energy decrease. Considering the structure transformations shown in Figure 2, it is concluded that the decrease of extra energy is the result of Pt-core/Au-shell formation. Furthermore, the transformation rate from other structures to Pt-core/Au-shell final structure depends strongly on the initial structure, the transformation path, and the composition of the initial clusters along with the rate of heating. It must be noted that we have used a very slow heating rate for this purpose. The Au-core/Pt-shell, and eutectic-like clusters have relatively

high structural energy and the Au and Pt atoms are in segregation state, which benefits the collective motion of the atoms, causing the formation of Pt-core/Au-shell structure relatively rapidly. On the other hand, the solid solution clusters transform to Pt-core/Au-shell at slower rate. For decahedra, Pt-core/Au-shell transformations display a comparatively small amount of energy decrease due to their smaller size than the others under study.

To clarify the dynamic process in a quantitative way, mean square displacements (MSDs) of the atoms in all the clusters are calculated by taking previous configurations in the recorded trajectory as reference configuration (see eq 1). During heating, the configurations were recorded at every 1 K interval.

$$\text{MSD} = \langle |\mathbf{r} - \mathbf{r}_{\text{ref}}|^2 \rangle \quad (1)$$

where  $\mathbf{r}$  is the current position vector of the atom,  $\mathbf{r}_{\text{ref}}$  is the position vector of the atom in the reference configuration, and  $\langle \rangle$  denotes averaging over all the atoms. In this manner, the MSDs reflect the relative change of diffusivity of the atoms at different temperatures more directly. The calculated MSDs for cuboctahedra of solid solution, eutectic-like, Au-core/Pt-shell, and Pt-core/Au-shell structures are presented in Figure 4. The MSDs are calculated for whole cluster, along with the components Au and Pt. The dynamic melting process and its mechanism could be revealed better from the MSDs. Though different features in the energy curves (Figure 3) near melting are observed due to melting and elemental redistribution, the MSDs of the two elements reveal very similar feature, a steep increase of MSD with temperature, indicating the melting processes occur and finish within a small range of temperature. For solid solution, Au-core/Pt-shell and Pt-core/Au-shell, the Au and Pt melt simultaneously. However, for the eutectic-like cluster, it can be seen that the Au melts first and then Pt, which is in good agreement with the conclusion drawn in the structural analysis part. The curves in the rightmost panel of Figure 4, with different  $x$ -axis and  $y$ -axis scales than the others, are divergent due to the melting of the cluster above 800 K.

#### IV. Conclusions

Thermodynamic stability and melting behavior of Au–Pt nanoclusters of common structural variants like decahedra, icosahedra, and cuboctahedra were studied using molecular dynamics simulations. It has been observed that all these three types of structures have consistent stability orders. While the Pt-core/Au-shell structures are most stable, the eutectic-like

structures are more stable than solid solution ones, and the Au-core/Pt-shell are least stable. From the point of view of geometrical structure, the core/shell icosahedra and cuboctahedra are similarly stable, while eutectic-like and solid solution cuboctahedra are more stable than the same type of icosahedra. Large difference in melting points of the constituent elements acts as the dominating factor on the melting mechanism of the bimetallic nanoparticles. It has been demonstrated that on heating, the bimetallic clusters transform to the most stable Pt-core/Au-shell structure from other structural forms at certain temperatures.

#### References and Notes

- (1) Luo, J.; Njoki, P. N.; Lin, Y.; Mott, D.; Wang, L. Y.; Zhong, C. J. *Langmuir* **2006**, *22*, 2892.
- (2) Luo, J.; Maye, M. M.; Kariuki, N. N.; Wang, L. Y.; Njoki, P.; Lin, Y.; Schadt, M.; Naslund, H. R.; Zhong, C. J. *Catal. Today* **2005**, *99*, 291.
- (3) Luo, J.; Njoki, P. N.; Lin, Y.; Wang, L. Y.; Zhong, C. J. *Electrochem. Commun.* **2006**, *8*, 581.
- (4) Maye, M. M.; Kariuki, N. N.; Luo, J.; Han, L.; Njoki, P.; Wang, L. Y.; Lin, Y.; Naslund, H. R.; Zhong, C. J. *Gold Bull.* **2004**, *37*, 217.
- (5) Luo, J.; Maye, M. M.; Petkov, V.; Kariuki, N. N.; Wang, L. Y.; Njoki, P.; Mott, D.; Lin, Y.; Zhong, C. J. *Chem. Mater.* **2005**, *17*, 3086.
- (6) Nakanishi, M.; Takatani, H.; Kobayashi, Y.; Hori, F.; Taniguchi, R.; Iwase, A.; Oshima, R. *Appl. Surf. Sci.* **2005**, *241*, 209.
- (7) Cao, L. Y.; Tong, L. M.; Diao, P.; Zhu, T.; Liu, Z. F. *Chem. Mater.* **2004**, *16*, 3239.
- (8) Garcia-Gutierrez, D.; Gutierrez-Wing, C.; Miki-Yoshida, M.; Jose-Yacamán, M. *Appl. Phys. A: Mater. Sci. Process.* **2004**, *79*, 481.
- (9) Tada, H.; Suzuki, F.; Ito, S.; Kawahara, T.; Akita, T.; Tanaka, K.; Kobayashi, H. *ChemPhysChem* **2002**, *3*, 617.
- (10) Toshima, N.; Hirakawa, K. *Polym. J.* **1999**, *31*, 1127.
- (11) *Binary Alloy Phase Diagrams*; Massalski, T. B., Okamoto, H., Subramanian, P. R., Kacprzak, L., Eds.; American Society of Metals: Materials Park, OH, 1990.
- (12) Porter, A.; Easterling, K. E.; *Phase Transformations in Metals and Alloys*; Chapman and Hall: London, 1992; p309.
- (13) Liu, H. B.; Pal, U.; Medina, A.; Maldonado, C.; Ascencio, J. A. *Phys. Rev. B* **2005**, *71*, 075403.
- (14) Ascencio, J. A.; Liu, H. B.; Medina, A.; Pal, U. *Microscopy Res. Tech.* **2006**, *69*, 522.
- (15) Liu, H. B.; Canizal, G.; Schabes-Retchkiman, P. S.; Ascencio, J. A. *J. Phys. Chem. B* **2006**, *110*, 12333.
- (16) Cai, J.; Ye, Y. Y. *Phys. Rev. B* **1996**, *54*, 8398.
- (17) Rose, J. H.; Smith, J. R.; Guinea, F.; Ferrante, J. *Phys. Rev. B* **1984**, *29*, 2963.
- (18) Banerjee, A.; Smith, J. R. *Phys. Rev. B* **1988**, *37*, 6632.
- (19) Johnson, R. A. *Phys. Rev. B* **1989**, *39*, 12554.
- (20) Riffkin, J. Center of Simulation, University of Connecticut, 2006, <http://www.ims.uconn.edu/centers/simul>.
- (21) Jose Yacamán, M.; Ascencio, J. A.; Liu, H. B. *J. Vac. Sci. Technol. B* **2001**, *19*, 1091.
- (22) <http://www.webelements.com/>.